THE ASTROPHYSICAL JOURNAL, 423:320–325, 1994 March 1

THE ROTATING MOLECULAR CORE IN G10.6−0.4: SYNTHESIS MAPS IN $^{12}C^{18}O$

PAUL T. P. HO
Harvard-Smithsonian Center for Astrophysics, 60 Garden Street, Cambridge, MA 02138
SUSAN TEREBEY
California Institute of Technology and Jet Propulsion Laboratory, IPAC 100-22, Pasadena, CA 91125
AND
JEAN L. TURNER
University of California, Department of Astronomy, 405 Hilgard Avenue, Los Angeles, CA 90024
Received 1993 January 25; accepted 1933 September 13

ABSTRACT

Using the Owens Valley Radio Observatory millimeter-wave interferometer, the compact molecular cloud core surrounding the H II region G10.60−0.4 has been resolved in the $C^{18}O$ $J = 1$–0 transition. Since this line is most likely optically thin, it is an excellent tracer of the total column density. We find a centrally condensed and flattened (12″.6 × 4″.2; 0.3 pc × 0.1 pc) core, which is rotating rapidly with a substantial velocity gradient (17 ± 2 km s^{-1} pc^{-1}) along the major axis. The core is quite bright (>10 K), dense (>10^6 cm^{-3}), massive (10^3 $M_\odot$), and embedded in a more extended (>60″) envelope. There is no evidence for absorption, implying that the $C^{18}O$ emitting gas is both optically thin and substantially hotter than the equivalent continuum temperature at 3 mm. The systemic velocity of the rotating core is -2.5 ± 0.5 km s^{-1}, the same as the systemic velocity of the extended cloud.

Subject headings: ISM: individual (G10.6−0.4) — ISM: kinematics and dynamics — ISM: molecules

1. INTRODUCTION

The star-forming complex G10.6−0.4 is located at a distance of about 6 kpc (Downes et al. 1980) with a far-infrared luminosity of 10^6 $L_\odot$ (Fazio et al. 1978). This complex consists of a cluster of OB stars (Ho & Haschick 1981; Ho, Klein, & Haschick 1986). Toward the brightest H II condensation, a rapidly rotating core (10 km s^{-1} pc^{-1}) was found in NH_3 emission. Furthermore, a component of the NH_3 material, redshifted by ≈3–5 km s^{-1}, was found in absorption projected against the H II knot G10.6−0.4A (Ho & Haschick 1986). This redshifted absorption feature was interpreted as infalling material which continues to accrete toward the central star even after it has arrived on the main sequence. The suggestion was made that this infall and the rapidly rotating motions are related as might be expected in the case of spin-up which accompanies contraction.

Although contraction of cloud material must occur in forming a star, the observational evidences for actual contraction are scant. This is due to the short duration of the contraction phase, the small spatial scale of the phenomenon, and the relatively cool and nonluminous state of the material before the central star is formed. To further define the infalling material in G10.6−0.4, a series of studies were pursued with higher angular resolution (<1″), and with different NH_3 transitions. These studies showed that the redshifted component appears to be more optically thick, hotter, and denser than the surrounding rapidly rotating core, (Keto, Ho, & Haschick 1987a, 1988). This is consistent with the idea that the infalling material is the inner portion of the rotating core which is closer to the central heating source. At 1″ resolution, the absorption projected against the H II knot is resolved. The kinematics shows a curved structure in a position-velocity diagram. This was interpreted as evidence that the infalling motions must occur very close to the H II region so that projection effects are detectable across the H II region. On this point, alternative interpretations have been offered based on H_2CO observations (Guilloteau et al. 1988) and CS observations (Omodaka et al. 1992) which suggest that the infalling material may consist of fragments which are rotating with respect to each other. In the meantime, a few other candidates of contraction have been proposed (W49: Welch et al. 1987; W51: Rudolph et al. 1990; W3(OH) and G34: Keto, Ho, & Reid 1987b).

In this paper, we report $C^{18}O$ observations of the rotating core in G10.6−0.4. Previous investigations focused on spectral lines that were optically thick or had hyperfine structure, thus complicating the interpretation of the data. However, this rare isotope of CO is optically thin and is a reliable tracer of the total column density. We used interferometry to achieve the necessary high angular resolution (6″ = 5.4×10^{17} cm = 0.17 pc). By using an optically thin tracer we can measure the mass and determine unambiguously the central velocity of the system. The aim is to verify that the kinematics is independent of the chemistry and to further test the dynamical picture outlined above.

2. OBSERVATIONS

The interferometric observations of the $J = 1$–0 $C^{18}O$ line at 109.78 GHz were made with the millimeter wavelength interferometer at the Owens Valley Radio Observatory. Six tracks were obtained with the three-element interferometer in five different configurations between 1986 November and 1987 April. The range of baselines sampled is from 15 m to 85 m. Projection of baselines provided further information down to 10 m spacings. With uniform weighting of the (u, v) data, an angular resolution of 7″.5 × 5″.4 was achieved. With only a single pointing of the telescope, the largest structure that this experiment is sensitive to is limited not only by the primary beam response of 68″ but also by the absence of short spacings. Structures larger than 30″ will be attenuated by more than 65%. Flux calibration was referred to Mars and Uranus, while

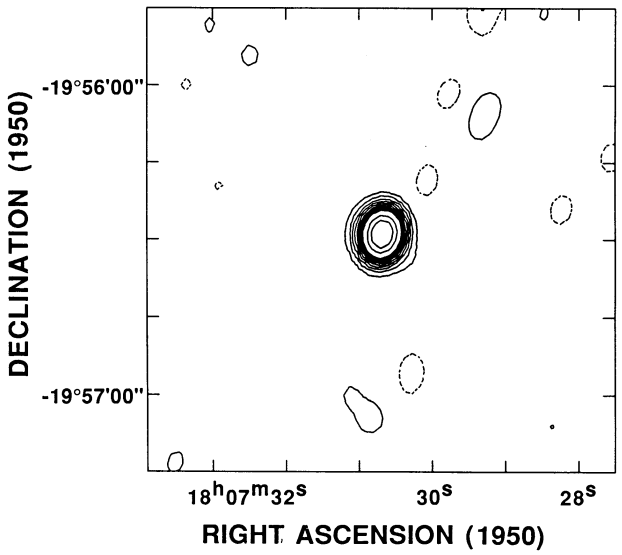

FIG. 1.—Continuum map at 2.7 mm for G10.6−0.4. The contour levels are: −2, −1, 1, 2, 3, 4, 5, 6, 7, 8, 9, 10, 15, and 20 × (100 mJy beam^{-1}). The synthesized beam is 7″.5 × 5″.4. The fluxes have not been corrected for primary beam (68″) attenuation. Note that the continuum map has been constructed from off-line emission and is uncontaminated by $C^{18}O$ emission.

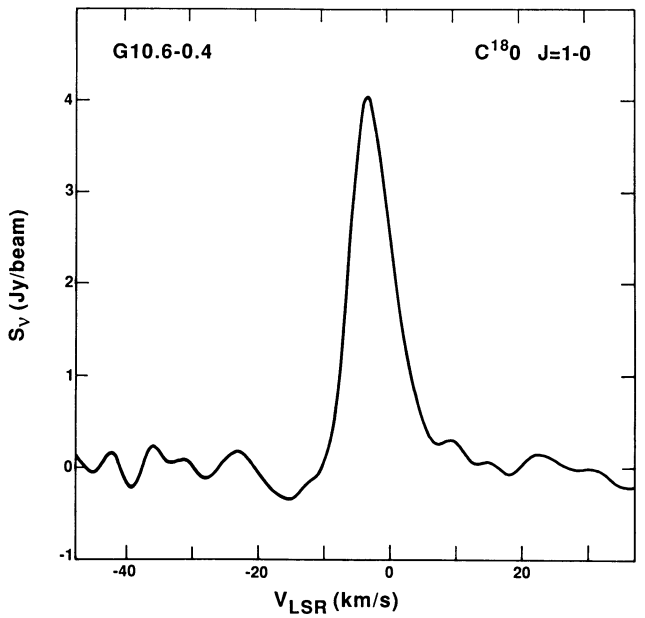

FIG. 2.—Observed spectrum of $C^{18}O$ emission toward the continuum peak: R.A.(1950) = 18^{h}07^{m}30^s.7, Decl.(1950) = −19°56′30″. The continuum emission has been subtracted from the spectrum. Note that there is no hint of absorption.

phase calibrations made use of nearby quasars. The accuracy of absolute flux calibration is about 15% (1 σ). Based on phase noise, the absolute positional accuracy of our maps is about 1″. For the spectroscopy, a total bandwidth of 32 MHz was sampled with 1 MHz resolution corresponding to 2.7 km s^{-1} resolution. The achieved rms noise was about 0.10 Jy per beam, or 0.25 K in brightness referred to the synthesized beam.

In Figure 1, we show a continuum map of the region constructed from the spectral channels away from the line emission (−47.3 to −14.6, and 15.5 to 37.3 km s^{-1}). We detect essentially only the brightest continuum component G10.6−0.4A (Ho & Haschick 1981), and not any of the other secondary condensations. The peak flux of 2.8 Jy is consistent with the peak flux of 2.4 Jy measured at 1.3 cm with a 3″ beam (Keto et al. 1988). The nondetection of the secondary condensations is consistent with their reported intensities at 1.3 cm and their optically thin emission. In Figure 2, we show a spectrum of the $C^{18}O$ emission toward the continuum peak. The flatness of the baseline suggests that the continuum emission has been removed properly. There is no obvious absorption feature as is seen in the NH_3 lines (e.g., Ho & Haschick 1986; Keto et al. 1987a). The peak flux of 4.0 Jy beam^{-1} corresponds to a brightness temperature of 10 K referred to the 7″.5 × 5″.4 beam. In Figure 3, we show the individual channel maps of the $C^{18}O$ emission. By comparing the spatial distribution as a function of velocity, we can see that there is a velocity gradient across the source. In Figure 4, we show the integrated intensity. The emission is extended north–south, but the most intense core shows a flattened structure oriented in the southeast–northwest direction. Simultaneously fitting two Gaussian components for the core and the envelope, we derive the following properties for the core: 22.8 ± 1.4 Jy beam^{-1} km s^{-1} for peak integrated flux, 63.9 ± 4.0 Jy beam^{-1} km s^{-1} for total integrated flux, (12″.6 ± 0″.6) × (4″.2 ± 0″.8) for the deconvolved size, and 110° ± 6° for the P.A. of the major axis. By rotating the data cube, position-velocity diagrams were made at 10° intervals relative to the right ascension and declination axes. The direction of maximum velocity gradient can be determined to within 20° accuracy and is essentially along the major axis of the flattened core shown in Figure 4. Position-velocity diagrams along P.A. = 120° and 30° are shown in Figure 5. A well-defined velocity gradient of 17 km s^{-1} pc^{-1} is seen in the direction of the major axis. In contrast, along the minor axis, a velocity gradient is not detected within the FWHM extent of the core. However, note that by including the emission outside the half-intensity contour of the minor-axis plot, a gradient appears to be present. This is due to the presence of envelope emission which is more extended in the minor axis direction. Both the magnitude and direction of the velocity gradient in the flattened core are consistent with the values reported in the previous NH_3 studies (Ho & Haschick 1986; Keto et al. 1987a, 1988), as well as the CS studies (Omodaka et al. 1992).

3. DISCUSSION

3.1. *Rotating Core*

The key characteristics which define a rotating core should be (1) a clearly defined velocity gradient, (2) a flattened cloud morphology where the elongation is parallel to the velocity gradient as to be expected in rotation, (3) a column density distribution consistent with central condensation, (4) a mass estimate which is consistent with gravitational binding. We will address these considerations here with regard to G10.6−0.4.

Via Figure 5, one can see that there is a well-defined velocity gradient of 17 ± 2 km s^{-1} pc^{-1} in the flattened $C^{18}O$ core. This is consistent with the earlier results in NH_3, which showed that within the slowly rotating (1 km s^{-1} pc^{-1}) and extended envelope, there is a rapidly roating (10 km s^{-1} pc^{-1}) and compact (0.4 pc radius) core (Ho & Haschick 1986). A major axis was not as well defined in the NH_3 emission, because of the presence of strong absorption against the H II

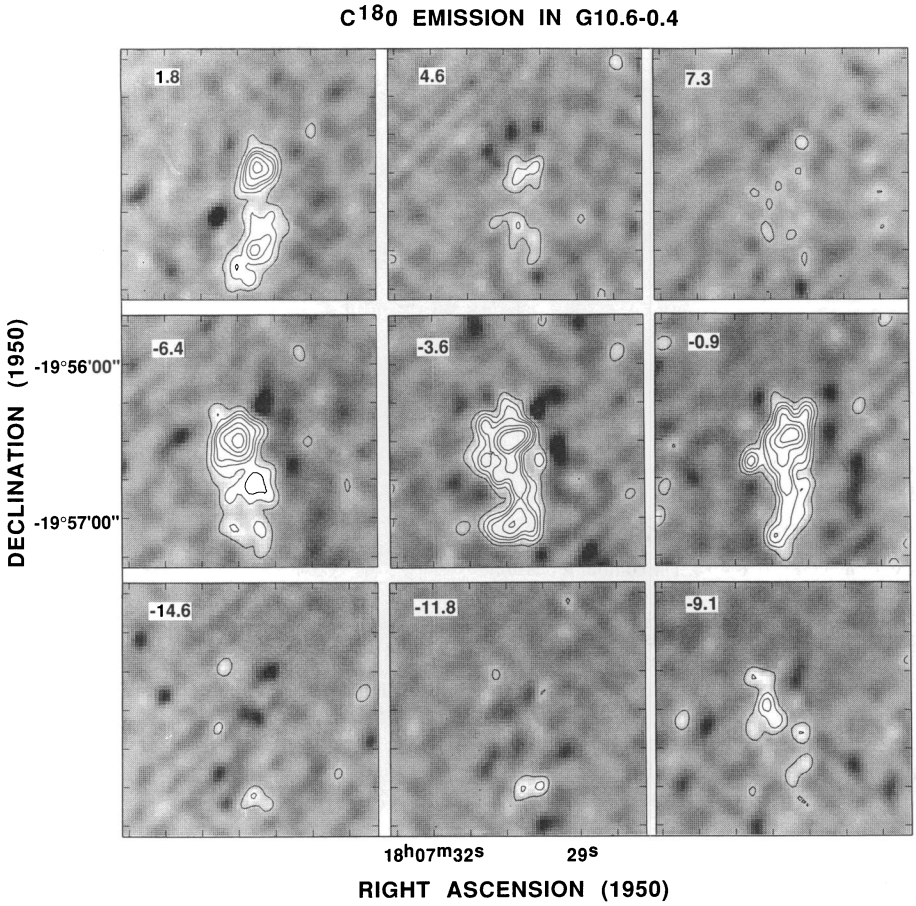

FIG. 3.—Contour maps for nine velocity channels of the $C^{18}O$ emission. The emission velocity of each channel is as indicated. Contour levels are: 1, 2, 3, 4, 6, 8, 10 × (300 mJy beam^{-1}; 0.75 K). The synthesized beam is as in Fig. 1. The superposed gray-scale image ranges from −0.6 to 0.6 Jy beam^{-1} and reflects the noise structures in the maps. These maps have not been corrected for the primary beam attenuation. Note that again there is no hint of absorption. In the NH_3 observations of Ho & Haschick (1986), the absorption feature spanned the velocity range of −3 to 2 km s^{-1}.

region. Hence, the velocity gradient measured in NH_3 was along the right ascension axis, 30° offset from the major axis determined here, and thereby underestimating the actual velocity gradient. Higher velocity gradients, by a factor of about 3, had been inferred for the inner region (0.05 pc radius) of this compact core, from high-resolution absorption line studies (Keto et al. 1988). The picture therefore appears to be consistent with spin-up motions, where the rotational velocity increases as we go to smaller spatial scales.

Via Figure 4, we confirm that, as seen in $C^{18}O$, the rapidly rotating core is indeed embedded in a lower density structure. Note in particular how well the core stands out against the weaker emission of the envelope. This has not been seen with such clarity in heretofore observations in NH_3 and CS. Several points are worthy of note: (1) the compact core is highly flattened and barely resolved in the minor axis, (2) the orientation of the major axis of the compact core is in the same direction as the maximum velocity gradient seen in Figure 5, (3) the compact core is 1.4 times stronger than the underlying envelope in terms of the peak integrated flux, and is about a factor of 5 smaller than the envelope in terms of total integrated flux over 30″ (although this is a lower limit since the envelope emission is suppressed by the lack of short spacings), (4) the peak of the $C^{18}O$ emission is located at R.A.(1950) = $18^h07^m30^s.6$, Decl.(1950) = 19°56′29″, which is coincident with the peak of the continuum emission to within the pointing and fitting accuracies.

3.2. *Absence of Absorption*

The fact that neither the integrated $C^{18}O$ emission nor the individual velocity channels show any evidence of absorption, the fact that the integrated emission is centrally peaked on the continuum source, and the fact that the envelope emission can be seen very well are all extremely important new findings. In contrast to the NH_3 observations (e.g., Ho & Haschick 1986) and CS observations (Omodaka et al. 1992), where the integrated emission shows a distinct depression toward the continuum peak, the $C^{18}O$ does not. We note that this is not due to a beam effect since the synthesized beam is in fact smaller in this experiment as compared to these previous data sets.

At first glance, the absence of absorption appears to support the model that the bulk of the gas must lie behind the H II region (Guilloteau et al. 1988). However, the likeliest explanation for the absence of absorption is probably the weakness of the continuum temperature as compared to the neutral gas temperature. Since the observed continuum flux at 3 mm is essentially the same as the value at 1.3 cm, we can conclude that it is optically thin. The brightness temperature of the con-

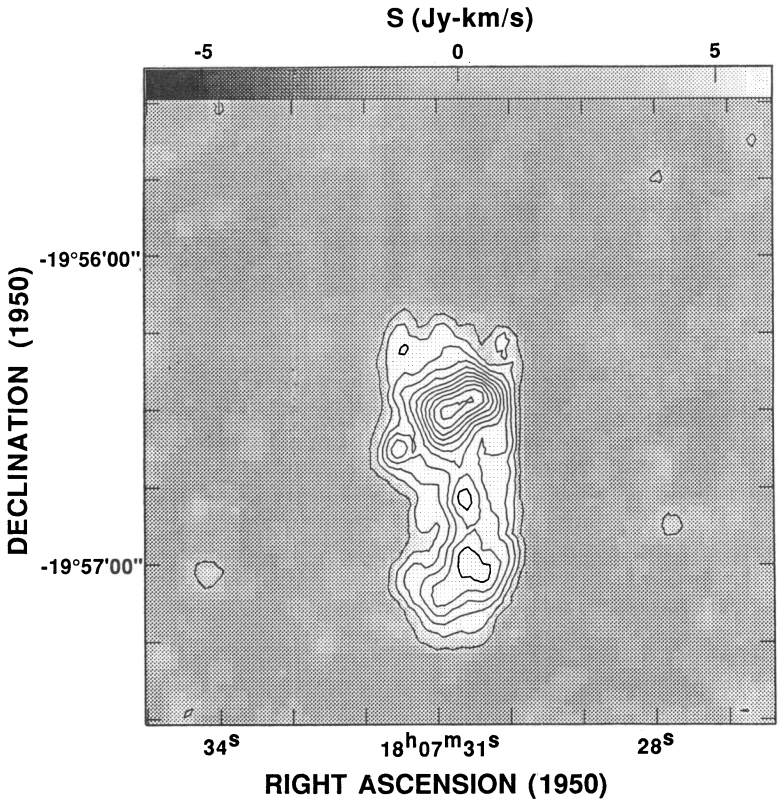

FIG. 4.—Contour map of the integrated intensity of the $C^{18}O$ emission. Contour levels are $-2, -1, 1, 2, 3, 4, 5, 6, 7, 8, 9, 10 \times (3.6$ Jy beam^{-1} km s$^{-1})$. Note that above the 50% contour, the emission shows a flattened structure oriented in the southeast–northwest direction. This flattened structure is centered on the peak of the continuum emission.

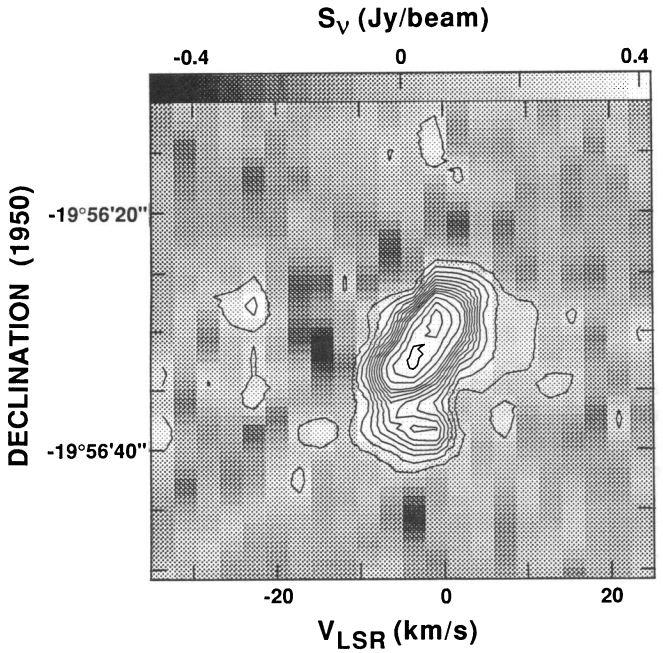

FIG. 5a

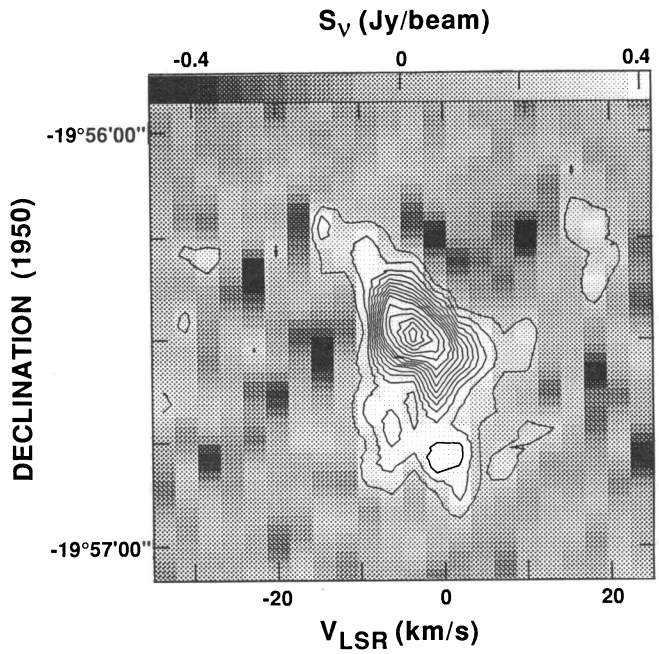

FIG. 5b

FIG. 5.—Position-velocity diagrams along the directions: (*a*) P.A. = 120° and (*b*) P.A. = 30°. These are approximately the P.A. for the major and minor axes of the flattened structure seen at the highest $C^{18}O$ intensities. Contour levels are: $-4, -3, -2, -1, 1, 2, 3, 4, 5, 6, 7, 8, 9, 10, 12, 14, 16, 18, 20, 25, 30, 40 \times (200$ mJy beam$^{-1})$. Note that along the major axis, a clear velocity gradient is seen at the highest intensities corresponding to the core of the cloud. Along the minor axis, a velocity gradient is not well-defined within the FWHM extent of the core of the cloud. Note that the lower intensity emission in both plots corresponds to the lower density and more extended envelope. In the case of the minor-axis cut, this introduces an apparent velocity gradient.

tinuum emission is then some 25 times lower at 3 mm as compared to 1.3 cm, being only 7.0 K referred to a 7".5 × 5".4 beam. Assuming the source size is 4" (Ho & Haschick 1981), the brightness temperature of the H II region at 3 mm is only 18 K. This is to be compared to the value of 700 K measured at 1.3 cm with 3" resolution. Thus, as a background source, the H II region is much hotter than the dense neutral gas (most likely 50–200 K) seen in NH_3 at 1.3 cm, but is probably cooler than the neutral gas seen in $C^{18}O$ at 3 mm. To illustrate this point we express in very simplified form the observed flux density along the line of sight to the H II region under the assumption that the line opacity is low:

$$B_\nu(T_B) = [\Omega_s(v)/\Omega_b][B_\nu(T_{ex}) - a(\Omega_{H\,II}/\Omega_b)B_\nu(T_{H\,II})]\tau(v) = 4.0 \text{ Jy},$$

where $\Omega_s(v)$ is the source size as a function of velocity, Ω_b is the beam size, $\Omega_{H\,II}$ is the size of the H II region, B_ν is the Planck function in flux density, a is the fraction of the cloud lying in front of the H II region (assumed to be 0.5 here), T_B is the observed brightness temperature, T_{ex} is the neutral gas temperature, and $T_{H\,II}$ is the temperature of the H II region. Since there is no sign of absorption at the 10% level, as a function of velocity or position, the simplest explanation would have the brightness temperature of the neutral gas dominating over that of the H II region, i.e., $T_{ex} \gtrsim 5(\Omega_{H\,II}/\Omega_b)T_{H\,II}$. For the synthesized beam, $(\Omega_{H\,II}/\Omega_b)B_\nu(T_{H\,II}) \sim 7.0$ K, hence a temperature $T_{ex} \gtrsim 35$ K is indicated. Further, since the continuum emission is comparable to the line emission away from the H II region, i.e., $(\Omega_{H\,II}/\Omega_b)B_\nu(T_{H\,II}) \sim B_\nu(T_{ex})\tau$, the line emission must be optically thin to keep the product $B_\nu(T_{ex})\tau$ at modest values, given that T_{ex} is substantial. From the above estimate of T_{ex}, $\tau \lesssim 0.1$.

If the neutral gas temperature does not greatly exceed the continuum temperature, there is one other possible explanation. Away from the H II region, when $\Omega_{H\,II}$ goes to zero, $B_\nu(T_{ex})\tau(v)$ will be comparable to $[B_\nu(T_{ex}) - (\Omega_{H\,II}/\Omega_b)B_\nu(T_{H\,II})]\tau(v_0)$, provided the decrease in $\tau(v)$ away from the central velocity v_0 is sufficiently fast to compensate for the absence of a background continuum.

Several pieces of information support these explanations for the absence of absorption at 3 mm: (1) in previous NH_3 studies, line opacities are highest at the absorption velocities, (2) the compact core as seen in $C^{18}O$ is quite small, especially in the minor axis, which means that the column density and hence opacity does decrease rapidly away from the H II region, (3) at 7 mm, where CS (1–0) observations were made by Omodaka et al. (1992), the continuum brightness temperature is higher than at 3 mm, and the CS emission is seen to be depressed toward the H II region although the observed brightness temperature are never negative. In addition, the CS was inferred to be quite optically thick. The CS observations were made with a somewhat larger 10".6 × 7".0 beam, and hence emission present within the beam may partially fill in the absorption against the H II region. Future observations with a smaller synthesized beam might detect enhanced absorption in CS and possibly in $C^{18}O$ as well.

Thus the absence of absorption in $C^{18}O$ suggests that this transition may be the best tracer of the total column density and the total mass, as compared to NH_3 and CS. Further, the detection of the somewhat fainter and much more extensive envelope emission suggests that this transition is not strongly biased by temperature, as to be expected for an optically thin line.

3.3. *Detected Mass*

From the measured integrated flux densities (see § 2), we can calculate the total column density for the flattened core in $C^{18}O$, CO, and H_2. For the normal isotope,

$$N_{CO} = 2.3 \times 10^{14} \text{ cm}^{-2}\left(\frac{T_{ex}^2}{T_0}\, e^{T_0/T_{ex}}\right)\left(\frac{\tau_{CO}}{1}\right)\left(\frac{\Delta V}{1 \text{ km s}^{-1}}\right).$$

Assuming an isotopic ratio $[^{16}O]/[^{18}O] = 500$, optically thin lines, and deriving $\tau_{C^{18}O}$ from the observed fluxes,

$$N_{CO} = 5.8 \times 10^{19} \text{ cm}^{-2}\left(\frac{T_{ex}}{50 \text{ K}}\right)^2 \times \left\{\frac{\int B_\nu[T_B(C^{18}O)]\delta V}{[B_\nu(T_{ex}) - a(\Omega_{H\,II}/\Omega_b)B_\nu(T_{H\,II})]1 \text{ km s}^{-1}}\right\}.$$

Thus, adopting a mean value $T_{ex} = 50$ K, neglecting $T_{H\,II}$ for the moment, the integrated $C^{18}O$ flux for the compact core corresponds to $N_{CO} = 2.0 \times 10^{20}$ cm^{-2}. Assuming [CO]/[H_2] abundance ratio of 10^{-4}, $N_{H_2} = 2.0 \times 10^{24}$ cm^{-2}. Assuming a disk geometry with a disk thickness equal to the deconvolved size of the minor axis, the volume density $n(H_2) = 2 \times 10^6$ cm^{-3}. The deduced mass for the compact core is $M(H_2) \sim 1100\ M_\odot$. This derived mass is somewhat underestimated by neglecting $T_{H\,II}$. To estimate whether the deduced mass is sufficient to bind the rotational motions, we find that if most of the mass is more or less spherically symmetric, the expected velocity gradient is 28 km s^{-1} pc^{-1}. Furthermore, if the density is approximately constant, the velocity gradient will be expected to be constant. These expectations are in good agreement with the observed velocity gradient, given the uncertainties in geometry and projection effects. The higher velocity gradient which is seen at smaller spatial scales is consistent with the idea that the column density probably increases toward the center where the effects of the stellar mass also become more important.

For the envelope, assuming a gas temperature $T_{ex} = 20$ K, the integrated flux over 30" yields a mass of 2500 $M_\odot$. The deduced volume density of the envelope is some 20 times lower than the compact core, $\sim 10^5$ cm^{-3}. If the gas temperature for the envelope is lower, the mass and density would be lower, scaling approximately linearly with temperature. If the path length of the envelope emission is greater, the volume density will also be reduced accordingly. The deduced mass for the envelope is underestimated by roughly a factor of 2 because of the missing short spacing flux.

3.4. *Fragmentation and Contraction*

Both Guilloteau et al. (1988) and Omodaka et al. (1992) have suggested that there may be substructures within this core. At the achieved resolution of 7".5 × 5".4, which is roughly 2 times finer in terms of beam area than the CS observations by Omodaka et al., we do not see substructure within the core. We surmise that this may be due to the fact that absorption may be more important in the CS observations than in the $C^{18}O$ observations. The optical depth of $C^{18}O$ is likely substantially lower than CS, and the continuum brightness temperature at 3 mm is much weaker than it is at 7 mm. The $C^{18}O$ may therefore be a better tracer of the total column density. Comparison with the OH and H_2CO observations of Guilloteau et al. is more problematical since our angular resolution is 170 times coarser in terms of beam area, while our velocity resolution is almost 3 times coarser. Hence we cannot comment on substructures at that size scale. What is clear, however, is that there is a lot of high-density material projected against the H II region and immediately surrounding it.

With regard to contraction as suggested by the NH_3 studies, our $C^{18}O$ data have not been too helpful since we do not

detect absorption. On the other hand, since absorption is not important, the mean velocity of the compact core can be deduced more accurately from the position-velocity diagrams. Figure 5 suggests that the mean velocity is close to -2.5 ± 0.5 km s^{-1}. This is in reasonable agreement with the value of -4 ± 1 km s^{-1} from high-resolution NH_3 absorption line studies, and the -5.5 ± 1.2 km s^{-1} from lower resolution NH_3 emission line studies. One should regard the present measurement as a much better estimate of the mean velocity of the compact core. This result does confirm that the absorption lines seen in NH_3, OH, H_2CO are redshifted with respect to the compact core. This result also suggests that the velocity of the CS ($J = 1$–0) emission toward the continuum peak, observed to be blueshifted with respect to the $C^{18}O$ and the $C^{34}S$ $J = 2$–1, may be influenced by weak redshifted absorption.

Furthermore the mean velocity of the extended $C^{18}O$ emission is the same as the -2.5 ± 0.5 km s^{-1} measured for the compact core. This value agrees well with the -3.0 km s^{-1} measured in $C^{34}S$ for the envelope (Omodaka et al. 1992).

Finally, it should be noted again that the compact cloud core is centered on the continuum H II region. To within the measurement error achieved in this experiment, the compact core as seen in $C^{18}O$ can be described as a flattened structure with a cluster of OB stars in the middle. If the OB stars and their H II regions were not embedded in the center of the cloud core, i.e., if they were located at the edge of the cloud core as suggested by Guilloteau et al. (1988), it would appear rather fortuitous that the $C^{18}O$ emission, which is optically thin and thereby traces the total column density, should be so well centered and symmetrical with respect to the H II region.

The new $C^{18}O$ results basically confirm the previous dynamical model for the region. The salient data from the high spatial resolution absorption experiments of Keto et al. (1988) and Guilloteau et al. (1988) show there is a pronounced velocity gradient across the H II region. The absorption peaks at roughly 1.0 km s^{-1} and is generally redshifted with respect to the -2.5 km s^{-1} center velocity of the compact core. The observed velocity gradient is difficult to explain by a pure contraction model. On the other hand, a pure rotation model has difficulty explaining why the peak absorption velocity is displaced from the systemic velocity of the compact core—unless the H II region is offset from the dynamical center. However, the data are very naturally explained by a model combining rotation and contraction (see, for example, Keto et al. 1988). If the H II region is at the dynamical center, then this model predicts a strong velocity gradient across the source. In addition, due to velocity crowding effects the peak absorption will be redshifted and spatially displaced from the dynamical center, which in this case occurs a few arcseconds northeast of the H II region emission peak. The new $C^{18}O$ results for the systemic velocity and spatial coincidence of the H II region with the center of the compact core support the picture of a flattened rotating structure that is contracting toward the central cluster of OB stars.

4. CONCLUSIONS

The molecular cloud core surrounding G10.6−0.4 was resolved by interferometric maps in the $C^{18}O$ $J = 1$–0 line. The core is found to be elongated ($12''.6 \times 4''.2$; 0.3×0.1 pc) and barely resolved in the minor axis direction. A large velocity gradient (17 ± 2 km s^{-1} pc^{-1}) is found along the major axis of the flattened structure, while little velocity gradient is seen along the minor axis. This is consistent with an interpretation that this is a flattened cloud core which has spun up upon contraction. From the measured column density, we deduce a mass of 1100 $M_\odot$ which is sufficient to gravitationally bind the observed motions. We did not detect absorption in the $C^{18}O$ line, which can be explained by the combination of a weak continuum brightness temperature as compared to the neutral gas temperature, and a strongly peaked column density as a function of velocity and distance from the H II region. Without detecting absorption, we cannot address the question of collapse. We do, however, obtain much better information on the compact cloud core. We find that the massive core is centered exactly, to within measurement errors on the order of 1″, on the continuum H II region. The mean velocity of the core is accurately measured to be -2.5 ± 0.5 km s^{-1}, which suggests that the absorption features seen in other transitions are redshifted with respect to the compact core. Taken together, these measurements suggest that the continuum complex G10.6−0.4 did form out of the compact cloud core. Part of the core appears to be still contracting toward the central stars.

We thank J. M. Torrelles for comments and discussions, and our referee for kind and helpful criticisms. P. T. P. H. is supported in part by NSF grants AST 87-20759 and NASA grant NAGW-3121. This work was carried out in part at the Jet Propulsion Laboratory, California Institute of Technology, under a contract with the National Aeronautics and Space Administration. Funding for the OVRO interferometer has been provided by NSF grant AST 90-16404.

REFERENCES

Downes, D., Wilson, T. L. Bieging, J., & Wink, J. 1980, A&AS, 40, 379
Fazio, G. G., Lada, C. J., Kleinmann, D. E., Wright, E. L., Ho, P. T.P., & Low, F. J. 1978, ApJ, 221, L77
Guilloteau, S., Forveille, T., Baudry, A., Despois, D., & Goss, W. M. 1988, A&A, 202, 189
Ho, P. T. P., & Haschick, A. D. 1981, ApJ, 248, 622
———. 1986, ApJ, 304, 501
Ho, P. T. P., Klein, R. I., & Haschick, A. D. 1986, ApJ, 305, 714
Keto, E. R., Ho, P. T. P., & Haschick, A. D. 1987a, ApJ, 318, 712
———. 1988, ApJ, 324, 920
Keto, E. R., Ho, P. T. P., & Reid, M. J. 1987b, ApJ, 323, L117
Omodaka, T., Kobayashi, H., Kitamura, Y., Nakano, M., & Ishiguro, M. 1992, PASJ, 44, 447
Rudolph, A., Welch, W. J., Palmer, P., & Dubrulle, B. 1990, ApJ, 363, 528
Welch, W. J., Dreher, J. W., Jackson, J. M., Terebey, S., & Vogel, S. N. 1987, Science, 238, 1550